Title: A subset of CD4+ effector memory T cells limit immunity to pulmonary viral infection and prevent tissue pathology via activation of latent TGFβ

McEntee CP[1,2,3*], Houston S[1,2,3], Finlay CM[1,2,3#], Rossi S[1,2,3], Liu G[4], Shaw TN[1,3†], Casulli J[1,2,3], Fife M[1,3], Smedley C[1,2,3], Griffith TS[5], Pepper M[6], Hussell T[1,3], Hansbro PM[4], Schwartz J-M[7], Paidassi H[8], Travis MA[1,2,3**]

1. Lydia Becker Institute for Immunology and Inflammation,

2. Wellcome Trust Centre for Cell-Matrix Research,

3. Division of Immunology, Immunity to Infection and Respiratory Medicine, Faculty of Biology, Medicine and Health, Manchester Academic Health Sciences Centre, University of Manchester, UK.

4. Centre for Inflammation, Centenary Institute and University of Technology Sydney, Faculty of Science, School of Life Sciences, Sydney, New South Wales, Australia.

5. University of Minnesota, Department of Urology, Center for Immunology, Minneapolis, MN, USA.

6. Department of Immunology, University of Washington School of Medicine, Seattle, WA, USA.

7. School of Biological Sciences, Faculty of Biology, Medicine and Health, University of Manchester, UK.

8. CIRI, Centre International de Recherche en Infectiologie, 'Normal and Pathogenic B cells' Team, Univ Lyon, Inserm U1111, Université Claude Bernard Lyon 1, CNRS UMR5308, ENS de Lyon, F-69007 Lyon France.

[*]Current address: School of Biochemistry and Immunology, Trinity Biomedical Sciences Institute, Trinity College Dublin, Dublin 2, Ireland

[#]Current address: Trinity Translational Medicine Institute, Trinity College Dublin, Dublin 2, Ireland

[†]Current address: Institute of Immunology and Infection Research, School of Biological Sciences, University of Edinburgh, Edinburgh, United Kingdom

****Corresponding author:** Mark A. Travis, 2.14b Core Technology Facility, Faculty of Biology, Medicine and Health, University of Manchester, Grafton Street, Manchester, M13 9NT, UK. E-mail: mark.travis@manchester.ac.uk Tel: +44 161 275 1701

Abstract

A rapid immune response to pathogen re-exposure underpins immunological memory, with protection against divergent pathogens such as heterologous or novel viral strains requiring cross-reactive memory T cells. Understanding the pathways that control memory T cell function is therefore important for the rational design of viral vaccines and will aid the discovery of therapies to boost anti-viral immunity. Here, we identify a sub-population of memory T cells that limit secondary immune responses to viral re-infection, which is crucial in preventing host tissue damage. We show that a population of $CD4^+$ effector memory T (T_{EM}) cells activate the important immunoregulatory cytokine TGFβ, via expression of an integrin, αvβ8. Integrin αvβ8 expression marks a transcriptionally distinct sub-population of $CD4^+$ T_{EM}, enriched for anti-inflammatory pathways. Loss of integrin αvβ8 on murine $CD4^+$ T_{EM}, but not $Foxp3^+$ regulatory T cells (T_{REG}), led to exacerbated virus-specific $CD8^+$ T cell responses following secondary influenza A virus (IAV) infection, which was associated with enhanced viral clearance. However, although accelerating clearance, loss of integrin αvβ8 expression on $CD4^+$ T_{EM} resulted in enhanced lung pathology following secondary IAV infection, which was completely reversed by adoptive transfer of $αvβ8^+$ $CD4^+$ T_{EM} cells. These data highlight a new pathway by which a distinct $CD4^+$ memory T cell subset restrains anti-viral immunity to prevent host tissue damage during secondary viral infection. Such pathways could be targeted therapeutically to either boost memory T-cell-mediated immunity or restrain host tissue damage during viral infection.

72 **Main text**

73 Whether induced by natural infection or vaccination, the development of robust
74 immunological memory is a cornerstone of sustained protective immunity against viruses,
75 either by directly targeting infected cells for killing or through the induction of high affinity,
76 virus-specific antibody responses. While viral surface proteins, the primary targets for
77 antibodies, can accumulate mutations over time leading to reduced antibody binding
78 affinity and neutralising efficacy, memory T cells typically recognise conserved epitopes
79 which are often shared between different viral strains or variants. Thus, virus-specific
80 memory T cells exhibit cross-reactivity to heterologous viruses, referred to as
81 heterosubtypic immunity, and are therefore a key component of long-lasting immunological
82 memory, particularly as viral variants emerge over time[1,2]. While the differentiation and
83 maintenance of memory T cells is highly dynamic, and functional/phenotypic plasticity
84 between subsets has been reported[3,4], traditionally they have been subdivided into three
85 major subsets based on their expression of homing markers and anatomical location.
86 Circulating $CD44^{high}$ memory T cells can be stratified into central or effector memory T cells
87 (T_{CM} or T_{EM} respectively) based on the expression or absence of markers including CD62L (L-
88 selectin) and CCR7 (C-C Motif Chemokine Receptor 7)[5]. $CD62L^{+}$ $CCR7^{+}$ T_{CM} migrate between
89 the circulation and secondary lymphoid structures whereas $CD62L^{-}$ $CCR7^{-}$ T_{EM} traffic
90 between lymphoid and peripheral tissues. In contrast, the third major memory T cell subset
91 reside predominantly in non-lymphoid peripheral tissues including the gastrointestinal tract,
92 skin and lung and are referred to as tissue-resident memory T cells (T_{RM})[6], although recent
93 data do suggest that T_{RM} populations can also leave the tissue and circulate[7]. Given their
94 importance in sustained, cross-reactive protective immunity against common pathogens,
95 understanding how memory T cells function is of fundamental importance, not only to aide

96 rational vaccine design, but also to identify targetable pathways for anti-viral
97 immunotherapies.
98
99 Here we show that a sub-population of $CD4^+$ T_{EM} control secondary immune responses to
100 respiratory viral infection by restraining the host T cell response. These cells are specialised
101 to activate the key immunoregulatory cytokine transforming growth factor-β (TGFβ) via
102 expression of the integrin αvβ8, exhibit an immune suppressive transcriptional profile, and
103 limit the frequency and cytotoxic potential of IAV-specific $CD8^+$ effector T cells during a
104 memory recall response. $CD4^+$ T_{EM} expressing integrin αvβ8 directly suppress $CD8^+$ T cells in
105 a TGFβ-dependent manner and are vital in preventing tissue pathology during secondary
106 infection. Additionally, we find that integrin αvβ8 is expressed by human $CD4^+$ T_{EM}, but no
107 other memory or naïve human $CD4^+$ or $CD8^+$ T cells, highlighting the potential of targeting
108 this pathway clinically to boost cytotoxic $CD8^+$ T cell responses in the context of anti-viral or
109 cancer immunotherapy. Together, our study uncovers a new suppressive role for a sub-
110 population of $CD4^+$ T_{EM} which express integrin αvβ8 and can activate latent TGFβ. These
111 properties make integrin $αvβ8^+$ $CD4^+$ T_{EM} key regulators of anti-viral memory T cell
112 responses and function to prevent inflammation-induced pathology following respiratory
113 viral infection.
114

115 **$CD4^+$ T_{EM} express *Itgb8* and activate latent TGFβ.**

116 A crucial cytokine in the regulation of many different immune cells, especially T cells, is
117 TGFβ[8]. TGFβ is initially secreted as a latent pro-form, consisting of the active moiety bound
118 non-covalently and encased by latency associated peptide (LAP), from which the active
119 cytokine must be liberated to function[9]. However, the role of TGFβ and its activation in
120 controlling the function of memory T cell responses is poorly understood.

121

122 To investigate whether TGFβ activation may play a role in regulating memory T cell function,
123 we first determined whether any memory T cell populations have the potential to activate
124 TGFβ. To this end, we assessed the expression of integrin αvβ8 on memory T cell subsets, a
125 molecule we and others have previously shown facilitates the activation of latent TGFβ by
126 immune cells[10]. To this end, we sorted multiple $CD4^+$ and $CD8^+$ splenic T cell populations
127 from Foxp3-YFP reporter mice[11] to assess expression of the gene encoding the integrin β8
128 subunit (*Itgb8*) across several subsets by qRT-PCR (gating strategy shown in Figure S1a). As
129 the integrin β8 subunit uniquely pairs with the αv subunit, this approach enabled us to
130 determine relative expression of integrin αvβ8. Interestingly, in addition to the expected
131 high levels of expression of *Itgb8* by $CD4^+$ $Foxp3^+$ T_{REG}[12], we also found for the first time that
132 $CD4^+$ T_{EM} ($CD44^{hi}$ $CD62L^-$) also expressed high levels of the gene (Figure 1a). In contrast,
133 *Itgb8* was not detected in naïve $CD4^+$ T cells ($CD44^{lo}$ $CD62L^+$) nor $CD4^+$ T_{CM} ($CD44^{hi}$ $CD62L^+$).
134 Similarly, all $CD8^+$ T cell subsets lacked expression of *Itgb8* (Figure 1a).

135

136 Next, to assess the expression of *Itgb8* at the single cell level, we utilised a novel dual
137 reporter mouse expressing GFP and tdTomato under control of the *Foxp3* and *Itgb8*
138 promoters respectively[13] (hereafter referred to as *Itgb8* reporter mice). We observed

139 expression of *Itgb8* in a subset of $CD4^+$ $T_{EM,}$ accounting for ~30% of the total $CD4^+$ T_{EM} pool
140 (Figure 1b-c). In contrast, no expression was detected in $CD4^+$ naïve or T_{CM} cells, or any $CD8^+$
141 T cell subsets (Figure 1b-c), consistent with our qRT-PCR data (Figure 1a). Additionally, we
142 also observed the presence of *Itgb8*-expressing $CD4^+$ T_{EM} at other anatomical locations,
143 including within non-lymphoid tissues such as the lung (Figure S1b-c) and intestine (Figure
144 S1d-e). Thus, the expression of *Itgb8* is unique to $CD4^+$ T_{EM} amongst the circulating memory
145 T cell pool.
146
147 Having determined that $CD4^+$ T_{EM} express *Itgb8*, we next investigated whether this enabled
148 these cells to activate latent TGFβ. To test this, we isolated $CD4^+$ T_{EM} from mice lacking *Itgb8*
149 expression on T cells (*Itgb8*$^{flox/flox}$ x CD4-Cre, hereafter called *Itgb8*$^{\Delta CD4}$ mice[14]) or their
150 littermate controls, and co-cultured them with an active TGFβ reporter cell line as previously
151 described[12]. We observed that $CD4^+$ T_{EM} activated latent TGFβ to levels comparable with
152 $CD4^+$ $Foxp3^+$ T_{REG} (Figure 1d). This ability to activate latent TGFβ was entirely dependent on
153 integrin αvβ8, as TGFβ activation was completely abrogated in $CD4^+$ T_{EM} cells isolated from
154 *Itgb8*$^{\Delta CD4}$ mice (Figure 1d). Taken together, these data show for the first time that $CD4^+$ T_{EM}
155 uniquely express *Itgb8* amongst the circulating memory T cell pool and can activate latent
156 TGFβ in an integrin αvβ8-dependent manner.
157
158 ***Itgb8*$^+$ CD4$^+$ T_{EM} exhibit a transcriptional profile associated with immune suppression.**
159 Although $CD4^+$ T_{EM} express *Itgb8* and can activate latent TGFβ, it is noteworthy that *Itgb8*
160 expression was not ubiquitous but rather restricted to a sub-population of $CD4^+$ T_{EM} (Figure
161 1b-c). These data could indicate stochastic expression within the population, or that
162 expression of *Itgb8* by $CD4^+$ T_{EM} is linked to a distinct phenotype or function compared to

163 their *Itgb8*-negative (*Itgb8*$^-$) counterparts. To investigate further, we purified *Itgb8*$^+$ and
164 *Itgb8*$^-$ CD4$^+$ T_{EM} from *Itgb8* reporter mice and performed bulk RNA-seq to directly compare
165 the transcriptome of the two populations. We found that the two populations showed a
166 profoundly different transcriptional profile, with 1599 significantly differentially expressed
167 protein coding genes (DEGs) between *Itgb8*$^+$ and *Itgb8*$^-$ CD4$^+$ T_{EM} with a Log_2 fold change
168 greater than 0.5 (Figure 1e, Figure S2a-b, and Table S1). Amongst these DEGs were a
169 number of genes known to be associated with immune suppression or regulatory function,
170 including *Lag3*, *Tigit*, *Il10, Rnf128* and *Pdcd1*, which showed increased expression in *Itgb8*$^+$
171 T_{EM} relative to the *Itgb8*$^-$ subset (Figure 1f). These data suggest *Itgb8*$^+$ CD4$^+$ T_{EM} may
172 represent a suppressive population of memory T cells. Such a function would fit with
173 previous findings demonstrating that other immune cells capable of activating TGFβ via
174 integrin αvβ8, including dendritic cells (DCs)[14-18], T_{REGS}[12] and monocytes and macrophages[19],
175 are associated with immune suppressive or regulatory functions.
176
177 When sorting *Itgb8*$^+$ and *Itgb8*$^-$ CD4$^+$ T_{EM} from *Itgb8* reporter mice for RNA-seq analysis,
178 Foxp3$^+$ T_{REGS} were excluded based on their expression of GFP. However, as several of the
179 genes found to be up-regulated in *Itgb8*$^+$ CD4$^+$ T_{EM} are also associated with regulatory
180 immune responses, we performed a four-way bulk RNA-seq experiment to directly address
181 whether *Itgb8*$^+$ Foxp3$^-$ CD4$^+$ T_{EM} were transcriptionally similar to CD4$^+$ Foxp3$^+$ T_{REG}. Principle
182 component analysis (PCA) revealed each of the four CD4$^+$T cell subsets to be
183 transcriptionally distinct from one another (Figure 1g and Table S2). Unexpectedly, we
184 observed more variance based on *Itgb8* expression status (60%) than the difference
185 between T_{EM} and T_{REG} (Foxp3$^-$ and Foxp3$^+$; 30%) (Figure 1g), a feature confirmed by
186 correlating gene expression across groups (Figure S2c). Notably, expression of specific

187 suppressive genes was enriched in both *Itgb8*$^+$ Foxp3$^-$ T_{EM} and *Itgb8*$^+$ Foxp3$^+$ T_{REG} relative to
188 each of their respective *Itgb8*$^-$ counterparts (Figure 1h). However, although sharing some
189 suppression-related gene expression, there were clear differences in expression of other T
190 cell-associated genes (Figure S2d). Thus, these data show *Itgb8*$^+$ Foxp3$^-$ T_{EM} are
191 transcriptionally distinct from *Itgb8*$^+$ Foxp3$^+$ T_{REG} and identifies a Foxp3$^-$ memory T cell
192 subset with an immune-suppressive transcriptional profile.
193
194 **_Itgb8_$^+$ CD4$^+$ T_{EM} suppress IAV-specific CD8$^+$ memory T cell responses.**
195 Next, we sought to determine the functional importance of *Itgb8* expression by CD4$^+$ T_{EM} *in*
196 *vivo*, in the context of an antigen-specific recall response following secondary infection. To
197 this end, we utilised the well-characterised secondary influenza challenge model using
198 heterologous strains of IAV. Briefly, *Itgb8*$^{\Delta CD4}$ and littermate control mice were infected
199 intranasally with the IAV strain X31 (H3N2), allowed to recover for ~6 weeks, and then re-
200 challenged with the IAV strain A/PR/8 (H1N1, PR8) (Figure 2a). The magnitude of the anti-
201 viral T cell responses was tracked using major histocompatibility complex (MHC) class I- and
202 class II-restricted tetramers, which facilitated identification of IAV nucleoprotein (NP)-
203 specific CD8$^+$ and CD4$^+$ T cell responses, respectively (representative gating strategy shown
204 in Figure S3a). We found that, in comparison to littermate controls, by day 8 post-infection
205 *Itgb8*$^{\Delta CD4}$ mice had significantly enhanced IAV-specific CD8$^+$ T cell responses in the lung
206 following re-challenge with PR8, both in terms of frequency (Figure 2b-c) and absolute cell
207 numbers (Figure 2d), with similar increases observed in the lung-draining lymph nodes
208 (Figure S3b-c). In contrast, IAV-specific CD4$^+$ T cell responses were unaffected (Figure S3d-e).
209 Notably, no differences in the abundance of IAV-specific CD8$^+$ T cells were observed
210 following primary infection (Figure S3f-g), indicating *Itgb8* serves to restrain cytotoxic T

211 lymphocyte (CTL) responses following reactivation, rather than regulating their
212 differentiation following primary infection.

213 As both Foxp3^{+} T_{REG} and CD4^{+} T_{EM} express *Itgb8* (Figure 1a-c and [12]), a caveat of the
214 experiments using *Itgb8*$^{\Delta CD4}$ mice is that expression of the integrin is ablated on both T cell
215 subsets. Crucially however, the hyper-responsive IAV-specific CD8^{+} T cell phenotype we
216 observed following secondary IAV infection of *Itgb8*$^{\Delta CD4}$ mice is not due to a lack of *Itgb8*
217 expression in CD4^{+} T_{REG}, as deletion of *Itgb8* expression exclusively on Foxp3^{+} T_{REG}
218 (*Itgb8*$^{flox/flox}$ x Foxp3-Cre[12], herein called *Itgb8*$^{\Delta Foxp3}$ mice) exhibited no such phenotype after
219 IAV re-infection (Figure S3h-i).

220

221 Next, we analysed the effector profile of IAV-specific CD8^{+} T cells in *Itgb8*$^{\Delta CD4}$ mice following
222 secondary influenza challenge. In addition to being more abundant after secondary
223 infection, IAV-specific CD8^{+} T cells from *Itgb8*$^{\Delta CD4}$ mice exhibited heightened effector
224 properties, including enhanced production of granzyme B in the lung (Figure 2e-g) and lung-
225 draining LN (Figure S3j-k) and increased expression of genes encoding molecules associated
226 with cytotoxic T cell responses such as granzyme A (*Gzma*), granzyme B (*Gzmb*), perforin
227 (*Prf1*) and interferon gamma (*Ifng*) (Figure 2h-k).

228

229 Additionally, recent evidence suggests TGFβ is crucial in the formation of CD8^{+} T_{RM}, and that
230 activation of TGFβ by DCs and epithelial cells in an αv integrin-dependent manner promotes
231 the formation of T_{RM} at barrier sites such as the skin and intestine[20-22]. However, when we
232 analysed the development of IAV-specific CD8^{+} T_{RM} in the lung following secondary infection
233 (see materials and methods, and Figure S3a for gating strategy), this remained intact, and
234 was even elevated, in *Itgb8*$^{\Delta CD4}$ mice (Figure S3l).

235

236 Thus, taken together, these data suggest *Itgb8*$^{+}$ CD4^{+} T_{EM} have a suppressive phenotype and
237 dampen CD8^{+} T cell numbers and effector function *in vivo* during secondary viral infection.
238 Additionally, this cellular pathway of TGFβ activation is not involved in induction of CD8^{+} T_{RM}
239 in the lung, pointing to a dichotomy in functional outcomes depending on the cell type
240 responsible for the activation of TGFβ.

241

242 **_Itgb8_$^{+}$ CD4^{+} T_{EM} directly suppress Influenza virus-specific CD8^{+} memory T cell responses via**
243 **activation of TGFβ.**

244 Thus far, we have shown that deletion of *Itgb8* on T cells in *Itgb8*$^{\Delta CD4}$ mice results in
245 enhanced CD8^{+} T cell responses during secondary IAV infection. Furthermore, T cell
246 expression of *Itgb8* appears to be limited to CD4^{+} T_{EM} and CD4^{+} Foxp3^{+} T_{REG} (Figure 1a-c and
247 [12]), and mice lacking expression of *Itgb8* on Foxp3^{+} T_{REG} do not show any phenotype during
248 secondary IAV infection (Figure S3h-i). This strongly suggests that the enhanced IAV-specific
249 CD8^{+} T cell responses observed in *Itgb8*$^{\Delta CD4}$ mice is due to lack of *Itgb8* expression by CD4^{+}
250 T_{EM}. To prove this unequivocally and directly test the suppressive capacity of *Itgb8*$^{+}$ CD4^{+} T_{EM}
251 *in vivo*, we designed an experiment to assess whether *Itgb8*$^{+}$ CD4^{+} T_{EM} were sufficient to
252 reverse the enhanced IAV-specific CD8^{+} T cell responses in *Itgb8*$^{\Delta CD4}$ mice following
253 secondary IAV infection. To this end, we isolated *Itgb8*$^{+}$ and *Itgb8*$^{-}$ CD4^{+} T_{EM} from *Itgb8*-
254 reporter mice following resolution of primary X31 infection and adoptively transferred them
255 into convalescent *Itgb8*$^{\Delta CD4}$ mice prior to secondary PR8 infection (Figure 3a). We found that
256 although transfer of *Itgb8*$^{-}$ CD4^{+} T_{EM} had no effect, transfer of *Itgb8*$^{+}$ CD4^{+} T_{EM} completely
257 reversed the enhanced NP-specific CD8^{+} T cell response to IAV re-challenge seen in *Itgb8*$^{\Delta CD4}$
258 mice, to levels observed in littermate controls (Figure 3b-c). In addition, such an effect was

259 not limited to NP-specific CD8$^+$ T cells, as transfer of *Itgb8*$^+$ CD4$^+$ T_{EM} also efficiently
260 attenuated IAV polymerase (PA)-specific CD8$^+$ T cell responses in *Itgb8*$^{\Delta CD4}$ recipient mice to
261 levels seen in littermate controls, whereas transfer of *Itgb8*$^-$ CD4$^+$ T_{EM} had no such effect
262 (Figure S4a-b). Thus, these data show that *Itgb8*$^+$ CD4$^+$ T_{EM} cause suppressive effects *in vivo*
263 and are sufficient to reverse enhanced IAV-specific CD8$^+$ T cell responses in *Itgb8*$^{\Delta CD4}$ mice.
264
265 In light of these findings, we next sought to elucidate the mechanism(s) by which *Itgb8*$^+$
266 CD4$^+$ T_{EM} can suppress CD8$^+$ T cell responses after viral re-infection. As expression of *Itgb8*
267 by CD4$^+$ T_{EM} enables them to activate TGFβ (Figure 1d), and TGFβ can directly inhibit CD8$^+$ T
268 cells[23], we postulated that *Itgb8*$^+$ CD4$^+$ T_{EM} could directly suppress CD8$^+$ T cell responses via
269 their ability to activate TGFβ. To investigate this hypothesis, we performed an *ex vivo* CD8$^+$ T
270 cell proliferation assay and tested the ability of *Itgb8*$^+$ and *Itgb8*$^-$ CD4$^+$ T_{EM} to modulate the
271 proliferative response. To this end, we isolated *Itgb8*$^+$ and *Itgb8*$^-$ CD4$^+$ T_{EM} from *Itgb8*
272 reporter mice and co-cultured each of these subsets separately with Cell Trace Violet (CTV)-
273 labelled CD8$^+$ T cells that were activated with anti-CD3ξ and anti-CD28 antibodies. We found
274 that CD8$^+$ T cell proliferation was significantly inhibited when responder cells were co-
275 cultured with *Itgb8*$^+$, but not *Itgb8*$^-$ CD4$^+$ T_{EM} (Figure 3d-e). Furthermore, the inhibition of
276 CD8$^+$ T cell proliferation by *Itgb8*$^+$ CD4$^+$ T_{EM} was wholly dependent on active TGFβ, as this
277 inhibition was completely reversed when the cells were co-cultured in the presence of a
278 TGFβ blocking antibody (Figure 3d-e). Moreover, addition of exogenous, active TGFβ to co-
279 cultures of *Itgb8*$^-$ CD4$^+$ T_{EM} with CD8$^+$ responders also significantly reduced CD8$^+$ T cell
280 proliferation (Figure 3f-g), further implicating TGFβ as a key factor involved in immune
281 suppression mediated by *Itgb8*$^+$ CD4$^+$ T_{EM}.

282 Taken together, these data show that *Itgb8*$^{+}$ CD4^{+} T_{EM} restrain IAV-specific CD8^{+} T cells *in*
283 *vivo*, a function facilitated via their ability to activate TGFβ in an integrin αvβ8-dependent
284 manner, which can act directly on CD8^{+} T cells to inhibit their proliferation.
285
286 **_Itgb8_$^{+}$ CD4^{+} T_{EM} slow viral clearance but are vital in preventing lung pathology following**
287 **viral re-infection.**
288 We next sought to determine the physiological relevance of *Itgb8*$^{+}$ CD4^{+} T_{EM}–mediated
289 control of anti-viral memory T cell responses. To this end, we first analysed the ability of
290 *Itgb8*$^{\Delta CD4}$ mice and their littermate controls to clear the virus after secondary IAV infection.
291 We found that *Itgb8*$^{\Delta CD4}$ mice showed significantly more robust expulsion of the virus, with
292 reduced copies of viral RNA detected at days 5 and 8 post-secondary infection compared to
293 littermate controls (Figure 4a). In contrast, we did not observe any difference in the ability
294 of *Itgb8*$^{\Delta Foxp3}$ mice to clear viral load after secondary infection compared to littermate
295 controls (Figure S5a), providing strong evidence that the lack of *Itgb8* expression on Foxp3^{+}
296 T_{REG} is not responsible for the enhanced viral clearance in *Itgb8*$^{\Delta CD4}$ mice. Taken together,
297 our data indicate that *Itgb8*$^{+}$ CD4^{+} T_{EM}-mediated restraint of CD8^{+} T cells during secondary
298 IAV infection limits the ability of mice to rapidly clear the virus.
299
300 Our studies demonstrated a novel role for *Itgb8*-expressing CD4^{+} T_{EM} in restraining anti-viral
301 CTL responses and slowing clearance of the virus. We next wanted to determine the
302 functional importance of a pathway that essentially limits host immunity to pathogenic
303 challenge. Based on the potent cytotoxic profile of IAV-specific CD8^{+} T cells in *Itgb8*$^{\Delta CD4}$ mice
304 (Figure 2e-k), we hypothesised that this pathway may be important in limiting infection-
305 induced inflammation and lung pathology. Indeed, *Itgb8*$^{\Delta CD4}$ mice exhibited significantly

306 enhanced lung inflammation compared to littermate control animals after secondary
307 infection, with inflammatory cells locating around airways and blood vessels and infiltrating
308 the parenchymal area (Figure 4b-c). There was no difference in lung pathology between
309 *Itgb8*$^{\Delta CD4}$ mice and littermate controls after primary IAV infection (Figure S5b-c), again
310 indicating a role for *Itgb8*$^{+}$ CD4^{+} T_{EM} in controlling T cell responses during re-infection rather
311 than primary infection.
312
313 We next determined whether enhanced pathology observed after secondary IAV infection
314 in *Itgb8*$^{\Delta CD4}$ mice was directly due to the absence of *Itgb8*$^{+}$ CD4^{+} T_{EM}. To this end, we
315 analysed lung pathology following secondary IAV infection of *Itgb8*$^{\Delta CD4}$ mice that received
316 either *Itgb8*$^{+}$ or *Itgb8*$^{-}$ CD4^{+} T_{EM}. Transfer of *Itgb8*$^{+}$ CD4^{+} T_{EM}, but not *Itgb8*$^{-}$ CD4^{+} T_{EM},
317 completely reversed the enhanced lung pathology seen in *Itgb8*$^{\Delta CD4}$ mice after secondary
318 infection (Figure 4d-e), restoring histology and inflammation scores to that seen in control
319 mice (Figure 4b-c). Taken together, these data strongly indicate that although *Itgb8*$^{+}$ CD4^{+}
320 T_{EM} slow the ability of the host to clear viral load, they are essential in restraining
321 pathogenic anti-viral CD8^{+} T cell responses to prevent tissue pathology following re-
322 infection.
323
324 Having discovered that integrin αvβ8 expression identifies a sub-population of immune
325 suppressive murine CD4^{+} T_{EM}, which can restrain effector recall responses and prevent overt
326 inflammatory sequelae, we sought to determine whether a similar population might be
327 present in humans. To test this, we isolated human peripheral blood mononuclear cells
328 (PBMCs) and assessed expression of integrin αvβ8 on human T cell subsets by flow
329 cytometry using a monoclonal antibody specific for human αvβ8[15] (gating strategy shown in

330 Figure S6). In agreement with our pre-clinical data, expression of integrin αvβ8 was
331 restricted primarily to $CD4^+$ T_{EM} in human PBMCs (Figure 4f-g).
332
333 Together, our data for the first time show that a subset of cells classed as $CD4^+$ memory T
334 cells can be suppressive during re-infection. This suppressive function is reliant on their
335 expression of an integrin, αvβ8, which enables them to activate TGFβ. We find that these
336 cells are crucial in restraining $CD8^+$ T cell responses during re-infection with IAV in the lung
337 but are also present in the intestine. Thus, important future work will determine if these
338 cells have a broader function in regulating secondary immunity in other organs to a wide
339 range of challenges, or if the cells are specific to pulmonary immunity.
340
341 Our findings have important implications to how the immune system balances responses to
342 re-infection. Although immunological memory has evolved to promote more robust
343 responses to subsequent infections, it now appears that memory T cell subsets can also limit
344 the robustness of this response. In situations where re-infection is proving hard to
345 irradicate, it could be beneficial to inhibit the function of these suppressive memory T cells,
346 via blocking integrin αvβ8 and therefore the ability of these cells to activate TGFβ, to boost
347 $CD8^+$ T cell responses.
348
349 However, caution would be required with any such approaches, as these suppressive
350 memory T cells appear critical in limiting host pathology during re-infection. Thus, strategies
351 would have to balance the beneficial effects of promoting immunity to re-infection, with
352 potential tissue damage associated with an exacerbated response. A phase I clinical trial is
353 already underway in cancer using an antagonist of integrin αvβ8 to block TGFβ activation,

354 based on successful pre-clinical studies[24-26]. Based on our findings that this molecular
355 pathway is important in limiting tissue pathology to re-infection, attention to the infection
356 status of the patients during treatment periods may be prudent.
357
358
359

360 **Materials and methods**

361

362 ***Mice***

363 Conditional deletion of *Itgb8* (β8 integrin) expression specifically in T cells or T_{REG} was
364 achieved by crossing mice with a conditional floxed allele of *Itgb8* with CD4-Cre[14] or Foxp3-
365 YFP-Cre[12] mice. All mice were used for experiments at 8 to 12 weeks of age, with littermates
366 used as control. *Itgb8*-IRES-TdTomato mice, generated as previously described[13], were
367 provided by Dr. H. Paidassi and bred at the University of Manchester. All experiments were
368 approved under a project license granted by the Home Office UK, reviewed by the
369 University of Manchester Animal Welfare and Ethical Review Body and were performed in
370 accordance with the UK Animals (Scientific Procedures) Act of 1986. Mice were bred and
371 maintained in specific pathogen–free conditions at Bio Safety Level 2 with a 12-hour
372 light/dark cycle and food and water *ab libitum*.

373

374 ***Influenza A Virus Infections***

375 *Itgb8* conditional knockout mice and their littermate controls were anaesthetised with 2.5%
376 inhalable isoflurane and inoculated with 10^3 PFU of the IAV strain X31 (H3N2) or 10^1 PFU of
377 the IAV strain A/PR/8 (H1N1, PR8) intranasally, resulting in a transient infection and mild to
378 moderate weight loss. For secondary IAV challenge studies mice were inoculated with 10^3
379 PFU IAV-X31 and subsequently re-challenged ~6 weeks later with 10^1 PFU of the
380 heterologous strain IAV-PR8 and immune responses assessed at time-points indicated in the
381 figure legends.

382

383

384 ***Lung digest***

385 Lungs were transferred into 7 ml bijoux tubes containing 500 µl digestion mix consisting of 5
386 mg/ml collagenase I (Gibco) and 10 µg/ml DNase I (Sigma) in RPMI and finely minced with
387 scissors. An additional 1.5 ml of digestion mix was then added to samples and incubated in a
388 shaking incubator at 37°C for 40 minutes. Enzymes were quenched with ice-cold 10% RPMI
389 medium containing 10% FCS, and cells pelleted via centrifugation at 400 x g for 8 minutes.
390 Cell pellets were re-suspended in 2 ml red blood cell lysis buffer (Sigma) and washed with
391 ice-cold 10% FCS in RPMI prior to staining for flow cytometry.

392

393 ***Flow Cytometry***

394 Cell suspensions were transferred into 5 ml round bottom polystyrene tubes, washed in PBS
395 and stained with fixable viability Zombie dyes (Biolegend) diluted in PBS. Staining was
396 quenched by washing in FACS buffer (PBS with 2 mM EDTA and 2% FCS) after which cells
397 were incubated with anti-CD16/32 (Fc block, clone 2.4G2, BD Biosciences) for 15 minutes at
398 4°C to prevent non-specific binding. Without washing, antibodies specific for surface
399 markers were diluted in FACS buffer and added 1:1 directly onto samples and incubated for
400 a further 20 minutes at 4°C protected from light. Stained samples were then washed in PBS
401 and either re-suspended in FACS buffer for immediate sorting on a BD FACSAria™ cell sorter
402 or fixed using eBioscience™ Foxp3 / Transcription Factor Staining Buffer Set as per
403 manufacturer's guidelines. For experiments requiring T cell sorting, single cell suspensions
404 underwent a negative selection pre-enrichment using EasySep™ pan-T cell or memory $CD4^+$
405 T cell isolation kits as per manufacturer's guidelines (Stemcell™ Technologies).

406

407 To stain for intracellular markers or cytokines, fixed/permeabilsed samples were incubated
408 with antibodies diluted in 1X permeabilisation buffer. Samples were washed twice and re-
409 suspended in FACS-EDTA prior to acquisition on a BD LSR Fortessa™ or BD Symphony™.
410 Antibodies used for flow cytometry and FACS were purchased from Biolegend and/or
411 eBioscience™ and are listed in Supplementary Table 3.

412

413 To assess T_{RM} responses, intra-vascular labelling was performed as previously described[27].
414 Briefly, 3 µg anti-CD45.2 (104) conjugated to either FITC or APC was administered via i.v
415 injection into the tail vein in a final volume of 200 µl 3-5 minutes prior to performing
416 euthanasia. All flow cytometry data was analysed using FlowJo V10 software (Tree Star).

417

418 ***Tetramer Staining***

419 For assessment of Influenza virus-specific T cell responses, cells were transferred into 5 ml
420 round bottom polystyrene tubes, washed and incubated with Fc block for 15 minutes at
421 room temperature to prevent non-specific binding. Tetramers specific for $CD8^+$ T cells (H-
422 2D(b) Influenza A $NP_{366-374}$ (ASNENMETM) and H-2D(b) Influenza A $PA_{224-233}$ (SSLENFRAYV))
423 and $CD4^+$ cells (I-A(b) Influenza A $NP_{311-325}$ (QVYSLIRPNENPAHK)) recognising
424 immunodominant epitopes were obtained from the NIH tetramer facility at Emory
425 University and added at 5 µg/ml in RPMI and incubated for a minimum of 1 hour at 37°C
426 with regular agitation. Cells were washed in PBS and staining performed as described below
427 thereafter.

428

429

430

431 ***Quantitative PCR***

432 FACS-purified cells were sorted into complete media, washed in sterile PBS and re-
433 suspended in RLT buffer (Qiagen) containing 1% β-mercaptoethanol. For assessment of viral
434 mRNA in lung tissue a single lobe from the right lung was collected into a sterile 1.5 ml tube
435 containing RNA later and subsequently transferred into a 2ml tube containing RLT buffer
436 and a single 2 mm stainless steel bead. Tissue was homogenised into suspension using a
437 Qiagen Tissue Lyser. RNA was extracted from both cells and lysed tissue samples using
438 Qiagen RNeasy Mini Kit as per manufacturer's instructions. Reverse transcription of RNA to
439 cDNA was performed using the High Capacity RNA-to-cDNA Kit (Thermo Fisher Scientific)
440 and gene expression was assayed using PowerUp™ SYBR™ Green Master Mix (Applied
441 Biosystems). Reactions were run on a real-time PCR system (ABI 7500; Applied Biosystems).
442 Data for samples were normalized to *Gapdh* and are shown as a fold change compared with
443 the controls.

444

445 ***TGF-β Activation Assay***

446 FACS-purified T cell subsets were incubated overnight with a TGF-β reporter cell line[28] and
447 luciferase activity detected via the Luciferase Assay System (Promega). TGF-β activity was
448 determined as previously described[16].

449

450 ***RNA sequencing (RNA-seq)***

451 Total RNA was submitted to the Genomic Technologies Core Facility (GTCF) at the University
452 of Manchester and the quality and integrity of the RNA samples assessed using a 4200
453 TapeStation (Agilent Technologies) prior to the generation of libraries using the Illumina®
454 Stranded mRNA Prep. Ligation kit (Illumina, Inc.) according to the manufacturer's protocol.
455 Briefly, total RNA was used as input material from which polyadenylated mRNA was purified
456 using poly-T, oligo-attached, magnetic beads. Next, the mRNA was fragmented under
457 elevated temperature and then reverse transcribed into first strand cDNA using random
458 hexamer primers and in the presence of Actinomycin D (thus improving strand specificity
459 whilst mitigating spurious DNA-dependent synthesis). Following removal of the template
460 RNA, second strand cDNA was then synthesized to yield blunt-ended, double-stranded cDNA
461 fragments. Strand specificity was maintained by the incorporation of deoxyuridine
462 triphosphate (dUTP) in place of dTTP to quench the second strand during subsequent
463 amplification.

464

465 Following a single adenine (A) base addition, adapters with a corresponding,
466 complementary thymine (T) overhang were ligated to the cDNA fragments. Pre-index
467 anchors were then ligated to the ends of the double-stranded cDNA fragments to prepare
468 them for dual indexing. A subsequent PCR amplification step was then used to add the index
469 adapter sequences to create the final cDNA library. The adapter indices enabled the
470 multiplexing of the libraries, which were pooled prior to cluster generation using a cBot
471 instrument. The loaded flow-cell was then paired-end sequenced (76 + 76 cycles, plus
472 indices) on an Illumina HiSeq4000 instrument. Finally, the output data was demultiplexed
473 and BCL-to-Fastq conversion performed using Illumina's bcl2fastq software (v2.20.0.422).

474

475 ***RNA-seq data analysis***

476 The quality of the stranded paired-end RNA-seq reads were assessed using FastQC (v0.11.3;
477 https://www.bioinformatics.babraham.ac.uk/projects/fastqc/) and FastQ Screen (v0.13.0;
478 https://www.bioinformatics.babraham.ac.uk/projects/fastq_screen/), followed by adapter
479 removal and low-quality bases and reads trimming using BBDuk (BBMap suite v36.32;
480 http://sourceforge.net/projects/bbmap/). Processed reads were mapped against the mouse
481 reference genome (mm10) and gene annotation from Gencode (vM24) using STAR (v2.7.2b;
482 https://doi.org/10.1093/bioinformatics/bts635). The "--quantMode GeneCounts" option
483 was used to obtain read counts per gene from STAR.

484

485 Differential gene expression analysis was performed in the R environment using the
486 Bioconductor package DESeq2 (v1.30.1; https://doi.org/10.1186/s13059-014-0550-8).
487 Genes were considered significantly differentially expressed with a false discovery rate cut-
488 off of 0.05. The lfcShrink function (with apeglm method) was applied to produce a more
489 accurate log2 fold change estimates. The counts function (with normalized = TRUE) was
490 used to produce normalised counts, where it uses the median-of-ratios method to
491 determine scaling factors. Data transformation was performed using the rlog and vst
492 functions to obtain regularised logarithm and variance stabilizing transformation expression
493 values respectively. rlog transformed values were used to produce principal component
494 analysis plots using the prcomp function from the R package stats. vst values were used to
495 produce sample-to-sample correlation using the cor function from the R package stats.
496 Heatmaps and correlation plots were visualised using the R package pheatmap (v1.0.12).

497

498 ***T cell co-culture assays***

499 Spleens from *Itgb8*-IRES-TdTomato mice were manually dissociated, filtered through 40 µm
500 cell strainers and T cells enriched by negative selection using an EasySep™ pan-T cell
501 enrichment kit (Stemcell Technologies) as per manufacturer's guidelines. Splenic $CD4^+$ T_{EM}
502 and responder $CD8^+$ T cells from *Itgb8*-IRES-TdTomato mice were stained with cell surface
503 markers and further purified by FACS using a BD FACSAria™. $CD8^+$ T cells were subsequently
504 stained with CellTrace™ Violet proliferation dye (Thermo Fisher Scientific) and plated in a
505 1:1 ratio with *Itgb8*$^+$ or *Itgb8*$^-$ $CD4^+$ T_{EM} in RPMI containing 0.88 mM L-Glutamine (Gibco),
506 0.88 mM sodium pyruvate (Gibco), 0.04 mM β-mercaptoethanol, 0.88% (v/v) MEM non-
507 essential amino acids (Gibco), 0.35% (v/v) 100X MEM Vitamins (Gibco), 4.4 U/ml penicillin
508 (Gibco), 4.4 µg/ml streptomycin (Gibco) and 10% (v/v) heat-inactivated fetal calf serum
509 (FCS) (Sigma). Cells were added to sterile 96 well U-bottom tissue culture plates pre-coated
510 with purified NA/LE anti-CD3 (Clone 145-2C11) and soluble NA/LE anti-CD28 (Clone 37.51;
511 both BD Biosciences) added to provide co-stimulation. $CD8^+$ T cell proliferative responses
512 were measured after 72 hours by assessing dye dilution across cell divisions on a BD
513 Symphony™.

514

515 ***Adoptive transfer studies***

516 For adoptive transfer studies, *Itgb8*$^+$ or *Itgb8*$^-$ $CD4^+$ T_{EM} were FACS-purified from the spleens
517 of convalescent *Itgb8*-IRES-TdTomato mice and 2 x 10^5 of either cell type administered i.v
518 into the tail vein of IAV-X31 convalescent control or *Itgb8*$^{\Delta CD4}$ mice 1 day prior to re-
519 challenge with IAV-PR8.

520

521 ***Histological Assessment of Inflammation***

522 Mice were euthanised via intra-peritoneal injection of pentobarbitone and the thoracic
523 cavity opened to expose the lungs and trachea. The right lobes of the lungs were tied off
524 and removed for assessment of immune cell populations by flow cytometry. The remaining
525 left lobe was subsequently perfused with ~10 ml 1 mM EDTA in ice-cold PBS to remove
526 blood/circulating cells. The internal structure of the left lobe was then fixed by inflating with
527 1 ml 10% formalin via the trachea and the entire lobe subsequently immersed in 10%
528 formalin prior to transfer into 70% ethanol after 24 hours. Fixed lungs were embedded in
529 paraffin and sliced into 5 µm sections prior to staining with hematoxylin and eosin.
530 Histopathology was scored at 10x magnification of a light microscope according to a set of
531 custom-designed criteria to assess inflammation around airways, blood vessels and
532 parenchyma as previously described[29,30]. Six individual snapshots of each tissue section were
533 analysed in a blinded manner by two independent researchers and results collated.

534

535 ***Statistical Analysis***

536 Results are expressed as mean ± SEM. All statistical analysis was performed using GraphPad
537 Prism software (v9.4.1) and tests used are stated in the figure legends.

538

539

540

541

542

543

544

545

546

547

548 **Figure Legends:**

549 **Fig. 1| $CD4^+$ T_{EM} activate latent TGFβ via integrin αvβ8 and possess an immune suppressive**

550 **transcriptional profile.** a) Expression of *Itgb8* in FACS-purified murine splenic T cell subsets

551 as determined by RT-PCR (n=≥6). Statistical significance determined by one-way ANOVA

552 with Tukey's multiple comparisons ****p=≤0.0001, ns = not significant. b) Representative

553 flow cytometry plots of *Itgb8* expression in splenic $CD4^+$ (black) and $CD8^+$ (grey) T cell

554 subsets from *Itgb8*-reporter mice. c) Collated data of *Itgb8* expression on $CD4^+$ and $CD8^+$

555 splenic T cells at steady state. Data presented as frequency of *Itgb8*$^+$ cells as a percentage of

556 each parent population (n=8). Statistical significance determined by two-way ANOVA with

557 Tukey's multiple comparisons test ****p=≤0.0001, ns = not significant. d) Activation of

558 latent TGFβ by T_{REG} (n=3, Foxp3-YFP$^+$) or $CD4^+$ T_{EM} (n=6, $CD44^{hi}$ $CD62L^{lo}$ $Foxp3^-$) sorted from

559 the spleen of $Foxp3^{YFP}$ mice or mice with a conditional deletion of *Itgb8* on T cells (*Itgb8*$^{\Delta CD4}$).

560 Luciferase activity detected following overnight co-culture of each T cell subset with a TGFβ

561 responsive reporter cell line. Data from two independent experiments. Statistical

562 significance determined by Kruskall-Wallis with Dunn's multiple comparisons test *p=≤0.05,

563 ns = not significant. e) Volcano plot of relative expression from bulk RNA-seq (n=6) between

564 *Itgb8*$^-$ T_{EM} (left) and *Itgb8*$^+$ T_{EM} (right), with differential (Log_2 fold change > 0.5), statistically

565 significant genes (adjusted $p < 0.05$) indicated in red. f) Condensed heatmap of immune

566 suppressive genes differentially expressed between *Itgb8*$^+$ and *Itgb8*$^-$ T_{EM} from bulk RNA-seq

567 analysis (n=6). g) PCA of bulk RNA-seq experiment performed on flow cytometry-purified
568 splenic CD44^{hi} CD62L^{lo} Foxp3^{+} T_{REG} (*Itgb8*$^{+}$ versus *Itgb8*$^{-}$) and CD44^{hi} CD62L^{lo} Foxp3^{-} T_{EM} (*Itgb8*$^{+}$
569 versus *Itgb8*$^{-}$) (n = 3). h) Condensed heatmap of immune suppressive genes differentially
570 expressed between CD4^{+} *Itgb8*$^{+}$ and *Itgb8*$^{-}$ T_{EM} and T_{REG} (n = 3).
571
572 **Fig. 2| Conditional deletion of *Itgb8* on CD4^{+} T_{EM} enhances Influenza virus-specific CD8^{+} T**
573 **cell responses following heterologous secondary challenge.** a) Schematic of heterologous
574 secondary Influenza A Virus challenge protocol. Littermate control and *Itgb8*$^{\Delta CD4}$ mice were
575 infected with 10^{3} PFU IAV-X31 resulting in a transient, self-resolving infection. Six weeks
576 later, mice were re-challenged with 10^{1} PFU of the heterologous virus IAV-PR8 to facilitate
577 assessment of IAV-specific T cell responses. b) Representative flow plots of CD44^{hi} Influenza
578 nucleoprotein ($NP_{[366-374]}$)-specific CD8^{+} T cells in the lungs of littermate control and
579 *Itgb8*$^{\Delta CD4}$ mice 8 days following secondary infection with IAV-PR8 as determined by tetramer
580 staining (see Figure S3a for gating strategy). Frequencies shown are a percentage of total,
581 live CD45^{+}, single cells. c) Frequency and d) total number of NP-specific CD8^{+} T cells in the
582 lungs of littermate control and *Itgb8*$^{\Delta CD4}$ mice at indicated time-points following re-
583 challenge with IAV-PR8. Data (n=3-10 biological replicates) from three independent
584 experiments. Statistical significance determined by two-way ANOVA with Tukey's multiple
585 comparisons test ***p=≤0.001, *p=≤0.05, ns = not significant. e) Representative flow plots
586 of total CD8^{+} T cells producing Granzyme B in the lungs of littermate control and *Itgb8*$^{\Delta CD4}$
587 mice 5 days following secondary infection with IAV-PR8 as determined by tetramer and
588 intracellular staining. f) Frequency (as a percentage of total live CD45^{+} cells) and g) number
589 of Granzyme B-producing NP-specific CD8^{+} T cells in the lungs of littermate control and
590 *Itgb8*$^{\Delta CD4}$ mice 5 days following secondary infection with IAV-PR8 (n=8 biological replicates).

591 Statistical significance determined by Mann-Whitney test **p=≤0.01, *p=≤0.05. h-k) 1 x 10^5
592 NP-specific $CD8^+$ T cells were FACS-purified from the lungs of littermate control and
593 *Itgb8*$^{\Delta CD4}$ mice 5 days following secondary infection with IAV-PR8 and expression of h) *Gzma*,
594 i) *Gzmb*, j) *Prf1* and k) *Ifng* determined by RT-PCR (n=6 biological replicates from two
595 independent experiments). Statistical significance determined by Mann-Whitney test
596 **p=≤0.01, *p=≤0.05.

597 **Fig. 3| *Itgb8*$^+$ $CD4^+$ T_{EM} restrain anti-viral $CD8^+$ T cell responses following secondary**
598 **challenge and prevent $CD8^+$ T cell proliferation via TGFβ.** a) Schematic of $CD4^+$ T_{EM} adoptive
599 transfer study. Littermate control, *Itgb8*$^{\Delta CD4}$ and *Itgb8*-reporter mice were infected with 10^3
600 PFU IAV-X31. 6 weeks post-infection, *Itgb8*$^+$ and *Itgb8*$^-$ $CD4^+$ T_{EM} were purified by flow
601 cytometry from convalescent *Itgb8*-reporter mice and transferred intravenously into
602 convalescent *Itgb8*$^{\Delta CD4}$ recipients, 24 hours prior to heterologous re-challenge with 10^1 PFU
603 IAV-PR8. b) Representative plots of NP-specific $CD8^+$ T cells in the lungs of littermate control
604 and *Itgb8*$^{\Delta CD4}$ mice at day 8 post re-infection with IAV-PR8, the latter separated into two
605 cohorts based on having received either $CD4^+$ *Itgb8*$^+$ or *Itgb8*$^-$ T_{EM}. c) Frequency, as a
606 percentage of total live $CD45^+$ cells, of NP-specific $CD8^+$ T cells in the lungs of littermate
607 control and *Itgb8*$^{\Delta CD4}$ mice receiving either $CD4^+$ *Itgb8*$^-$ or *Itgb8*$^+$ T_{EM} at day 8 post re-
608 infection with IAV-PR8. Data (n=≥9) from three independent experiments. Statistical
609 significance determined by Kruskall-Wallis with Dunn's multiple comparisons test
610 **p=≤0.01, ns = not significant. d) Representative histograms of Cell Tracer Violet-labelled
611 naïve $CD8^+$ T cell, stimulated with anti-CD3 and anti-CD28 antibodies and co-cultured in a
612 1:1 ratio with *Itgb8*$^+$ or *Itgb8*$^-$ $CD4^+$ T_{EM} for 72 hours. Grey peaks represent $CD8^+$ T cells co-
613 cultured with *Itgb8*$^-$ $CD4^+$ T_{EM}, purple peaks signify $CD8^+$ T cells co-cultured with *Itgb8*$^+$ $CD4^+$
614 T_{EM} and green peaks represent $CD8^+$ T cells co-cultured with *Itgb8*$^+$ $CD4^+$ T_{EM} in the presence

615 of a TGFβ blocking antibody. e) Pooled data for frequency of $CD8^+$ T cells undergoing
616 proliferation under each condition in d (n=5 biological replicates from two independent
617 experiments). Statistical significance determined by one-way ANOVA with Tukey's multiple
618 comparisons test ***p=≤0.001, **p=≤0.01, ns = not significant. f) Representative histograms
619 and g) collated data of naïve $CD8^+$ T cell proliferative responses following co-culture in a 1:1
620 ratio with *Itgb8*$^-$ $CD4^+$ T_{EM} plus or minus recombinant TGFβ for 72 hours. Grey peaks/dots
621 represent $CD8^+$ T cells co-cultured with *Itgb8*$^-$ $CD4^+$ $T_{EM,}$ blue plots/dots represent $CD8^+$ T
622 cells co-cultured 1:1 with *Itgb8*$^-$ $CD4^+$ T_{EM} in the presence of recombinant TGFβ (n=5
623 biological replicates from two independent experiments). Statistical significance determined
624 by unpaired student's t-test ****p=≤0.0001.
625
626 **Fig. 4| Conditional deletion of *Itgb8* on $CD4^+$ T_{EM} facilitates rapid viral clearance but**
627 **induces significant tissue pathology.** a) Viral Matrix (M) protein mRNA in the lungs of
628 littermate control and *Itgb8*$^{\Delta CD4}$ mice at indicated time-points following re-challenge with
629 IAV-PR8 as determined by RT-PCR (n=≥4 biological replicates per-timepoint from two
630 independent experiments). Statistical significance determined by two-way ANOVA with
631 Šídák's multiple comparisons test ****p=≤0.0001. b) Representative images of H&E-stained
632 lung tissue sections from littermate control and *Itgb8*$^{\Delta CD4}$ mice 8 days following re-challenge
633 with IAV-PR8. c) Inflammation scores of blind-scored H&E-stained lung tissue sections from
634 littermate control and *Itgb8*$^{\Delta CD4}$ mice 8 days following re-challenge with IAV-PR8 (n=6
635 biological replicates). Statistical significance determined by Mann-Whitney test **p=≤0.01.
636 d) Representative images of H&E-stained lung tissue sections from *Itgb8*$^{\Delta CD4}$ mice 8 days
637 following re-challenge with IAV-PR8. 24 hours prior to re-challenge, *Itgb8*$^{\Delta CD4}$ mice were
638 adoptively transferred with either *Itgb8*$^-$ $CD4^+$ T_{EM} (grey) or *Itgb8*$^+$ $CD4^+$ T_{EM} (purple) purified

639 from convalescent *Itgb8*-reporter mice. e) Inflammation scores of blind-scored H&E-stained
640 lung tissue sections from *Itgb8*$^{\Delta CD4}$ recipient mice 8 days following re-challenge with IAV-
641 PR8. Statistical significance determined by Mann-Whitney test **p=≤0.01. f) Frequency of
642 integrin αvβ8-expressing cells amongst CD4^{+} and CD8^{+} T cell subsets in human PBMCs.
643 Frequencies shown are a percentage of total CD3^{+} cells (n=10 individual donors). Statistical
644 significance determined by two-way ANOVA with Tukey's multiple comparisons test. g)
645 Pairwise comparison of integrin αvβ8-expressing CD4^{+} and CD8^{+} T_{EM} in human PBMCs.
646 Statistical significance determined by two-tailed, paired student's t-test ****p=≤0.0001.
647
648
649
650
651
652
653
654
655
656
657
658
659
660
661
662

663

664

665

666

667

668

669 **Supplementary Figure Legends**

670

671 **Fig. S1| *Itgb8*-expressing CD4$^+$ T$_{EM}$ are present in non-lymphoid tissues.** a) Representative
672 gating strategy for analysing and sorting murine splenic T cell subsets. b) Representative
673 flow plots and c) collated data showing *Itgb8* expression in lung CD4$^+$ T cell subsets of *Itgb8*-
674 reporter mice. d) Representative flow plots and c) collated data showing *Itgb8* expression in
675 small intestinal CD4$^+$ T cell subsets of *Itgb8*-reporter mice. Data presented as frequency of
676 *Itgb8*$^+$ cells as a percentage of each parent population (n=3 biological replicates for each
677 tissue, representative of two independent experiments). Statistical significance determined
678 by two-way ANOVA with Tukey's multiple comparisons test ****p=≤0.0001, ns = not
679 significant.

680

681 **Fig. S2| *Itgb8*-expressing CD4$^+$ T$_{EM}$ and T$_{REG}$ possess a characteristic immune suppressive**
682 **transcriptional profile.** a) Heatmap of Z-scores of regularized variance stabilizing
683 transformed read counts from bulk RNA-seq (n=6) analysing CD4$^+$ *Itgb8*$^-$ T$_{EM}$ (left, black) and
684 CD4$^+$ *Itgb8*$^-$ T$_{EM}$ (right, red), with differential (Log$_2$ fold change > 0.5), statistically significant
685 (adjusted p < 0.05) genes indicated. b) Principal component analysis (PCA) of bulk RNA-seq
686 experiment performed on flow cytometry-purified splenic *Itgb8*$^+$ T$_{EM}$ versus *Itgb8*$^-$ T$_{EM}$ (n =

687 6). c) Sample similarity heatmap showing Pearson correlation between samples calculated
688 using regularized logarithmic (rlog)-transformed read counts. d) Heatmap of Z-scores of
689 regularized variance stabilizing transformed read counts of selected genes associated with T
690 cell biology.
691
692 **Fig. S3| Analysis of Influenza virus-specific T cell responses following primary and**
693 **heterologous secondary challenge in *Itgb8*$^{\Delta CD4}$ and *Itgb8*$^{\Delta Foxp3}$ mice.** a) Representative
694 gating strategy used to identify Influenza NP-specific CD8^{+} T cells, as well as tissue-resident
695 cells, in the lung of mice. b) Representative flow plots and c) collated data for the frequency
696 of CD44^{hi} Influenza NP-specific CD8^{+} T cells in the draining mediastinal lymph nodes of
697 littermate control and *Itgb8*$^{\Delta CD4}$ mice at indicated time-points post-secondary IAV-PR8
698 infection (n= ≥6 biological replicates from two independent experiments). Frequencies
699 shown are as a percentage of total CD8^{+} T cells per node. Statistical significance determined
700 by two-way ANOVA with Tukey's multiple comparisons test **p=≤0.01. d) Representative
701 flow plots and e) collated data for the frequency of CD44^{hi} Influenza NP-specific CD4^{+} T cells
702 in the lungs of littermate control and *Itgb8*$^{\Delta CD4}$ mice at indicated time-points post re-
703 challenge infection with IAV-PR8 (n=≥4 biological replicates per timepoint, from three
704 independent experiments). Frequencies shown are as a percentage of total, live CD45^{+},
705 single cells per lung. Statistical significance determined by two-way ANOVA with Tukey's
706 multiple comparisons test. f) Representative flow cytometry plots and g) collated data for
707 the frequency of NP-specific CD8^{+} T cells in the lungs of littermate control and *Itgb8*$^{\Delta CD4}$ mice
708 at indicated time-points post primary infection with IAV-PR8 (n=≥3 biological replicates per
709 timepoint representative of three independent experiments). Statistical significance
710 determined by two-way ANOVA with Tukey's multiple comparisons test. h) Representative

711 flow cytometry plots and i) collated data for the frequency of CD44^{hi} Influenza NP-specific
712 CD8^{+} T cells in the lungs of littermate control and *Itgb8*$^{\Delta Foxp3}$ mice at indicated time-points
713 following secondary infection with IAV-PR8 (n=10 biological replicates from two
714 independent experiments, n=3 for day 0 controls). Statistical significance determined by
715 two-way ANOVA with Tukey's multiple comparisons test. j) Representative flow cytometry
716 plots and k) collated data for frequency of Granzyme B-producing NP-specific CD8^{+} T cells in
717 the mediastinal lymph nodes of littermate control and *Itgb8*$^{\Delta CD4}$ mice at indicated time-
718 points post-secondary infection with IAV-PR8. Statistical significance determined by two-
719 way ANOVA with Tukey's multiple comparisons test **p=≤0.01. (n=≥4 biological replicates
720 from two independent experiments). Frequencies shown are as a percentage of total CD8^{+} T
721 cells per node. l) Frequency of intra-vascular (CD45.2 I.V+) and extra-vasculature (CD45.2-)
722 NP-specific CD8^{+} T cells in the lungs of littermate control and *Itgb8*$^{\Delta CD4}$ mice 8 days following
723 secondary infection with IAV-PR8, as determined by intra-vascular labelling and tetramer
724 staining (n=5 biological replicates from two independent experiments). Statistical
725 significance determined by two-way ANOVA with Tukey's multiple comparisons test
726 ****p=≤0.0001, *p=≤0.05.
727
728 **Fig. S4| *Itgb8*$^{+}$ CD4^{+} T$_{EM}$ restrain anti-IAV PA-specific CD8^{+} T cell responses following**
729 **secondary challenge.** a) Representative flow cytometry plots of viral polymerase (PA$_{[224-233]}$)-
730 specific CD8^{+} T cells in the lungs of littermate control and *Itgb8*$^{\Delta CD4}$ mice at day 8 post re-
731 infection with IAV-PR8, the latter separated into two cohorts on the basis of having received
732 *Itgb8*$^{+}$ or *Itgb8*$^{-}$ CD4^{+} T$_{EM}$ intravenously one day prior to re-challenge. b) Frequency, as a
733 percentage of total, live CD45^{+} single cells, of PA-specific CD8^{+} T cells in the lungs of
734 littermate control and both cohorts of *Itgb8*$^{\Delta CD4}$ mice at day 8 post re-infection with IAV-PR8

735 (n=≥9 biological replicates from three independent experiments). Statistical significance
736 determined by Kruskall-Wallis with Dunn's multiple comparisons test *p=≤0.05, ns = not
737 significant.
738
739 **Fig. S5| Expression of *Itgb8*$^{+}$ on Foxp3^{+} T_{reg} does not control viral titre and *Itgb8*$^{+}$ CD4^{+} T_{EM}**
740 **do not control lung pathology following primary IAV challenge.** a) Viral Matrix (M) protein
741 mRNA in the lungs of littermate control and *Itgb8*$^{\Delta Foxp3}$ mice at indicated time-points
742 following heterologous re-challenge with IAV-PR8 as determined by RT-PCR (n=3-5 biological
743 replicates per-timepoint). Statistical significance determined by two-way ANOVA with
744 Tukey's multiple comparisons test. b) Representative images of H&E-stained lung tissue
745 sections from littermate control and *Itgb8*$^{\Delta CD4}$ mice 6 weeks following primary infection with
746 IAV-PR8. c) Inflammation scores of blind-scored H&E-stained lung tissue sections from
747 littermate control and *Itgb8*$^{\Delta CD4}$ mice 6 weeks following primary infection with IAV-PR8 (n=4
748 biological replicates). Statistical significance determined by Mann-Whitney test.
749
750 **Fig. S6| Gating strategy for assessment of integrin αvβ8 expression of human T cell**
751 **subsets.** Representative gating strategy used to identify naïve T cells, T_{CM}, T_{EM} and T_{EMRA} in
752 human PBMC samples isolated from whole blood by Ficoll density gradient centrifugation.
753
754 **Table S1: Differentially expressed genes between *Itgb8*$^{+}$ and *Itgb8*$^{-}$ CD4^{+} T_{EM}.** List of 1599
755 differentially expressed protein-encoding genes between *Itgb8*$^{+}$ and *Itgb8*$^{-}$ CD4^{+} T_{EM} with a
756 Log_2 fold change greater than 0.5 and adjusted p-value of <0.05 (from RNA-seq experiment
757 shown in Figure 1e and Figure S2a-b).
758

759 **Table S2: Differentially expressed genes between *Itgb8*$^{+}$ and *Itgb8*$^{-}$ CD4+ T_{EM} and T_{REG}.** List

760 of differentially expressed protein-encoding genes from all possible two-way comparisons

761 between *Itgb8*$^{+}$ and *Itgb8*$^{-}$ CD4+ T_{EM} and T_{REG}, where a gene displayed a Log2 fold change

762 greater than 0.5 and adjusted p-value of <0.05 for any comparison (from RNA-seq

763 experiment shown in Figure 1g and Figure S2c-d).

764

765 **Table S3: List of flow cytometry antibodies and reagents used.**

766

767 **References.**

768 1 Altenburg, A. F., Rimmelzwaan, G. F. & de Vries, R. D. Virus-specific T cells as correlate of
769 (cross-)protective immunity against influenza. *Vaccine* **33**, 500-506 (2015).
770 https://doi.org:10.1016/j.vaccine.2014.11.054

771 2 Thomas, P. G., Keating, R., Hulse-Post, D. J. & Doherty, P. C. Cell-mediated protection in
772 influenza infection. *Emerg Infect Dis* **12**, 48-54 (2006).
773 https://doi.org:10.3201/eid1201.051237

774 3 Lees, J. R. & Farber, D. L. Generation, persistence and plasticity of CD4 T-cell memories.
775 *Immunology* **130**, 463-470 (2010). https://doi.org:10.1111/j.1365-2567.2010.03288.x

776 4 Omilusik, K. D. & Goldrath, A. W. Remembering to remember: T cell memory maintenance
777 and plasticity. *Curr Opin Immunol* **58**, 89-97 (2019).
778 https://doi.org:10.1016/j.coi.2019.04.009

779 5 Jameson, S. C. & Masopust, D. Understanding Subset Diversity in T Cell Memory. *Immunity*
780 **48**, 214-226 (2018). https://doi.org:10.1016/j.immuni.2018.02.010

781 6 Sasson, S. C., Gordon, C. L., Christo, S. N., Klenerman, P. & Mackay, L. K. Local heroes or
782 villains: tissue-resident memory T cells in human health and disease. *Cell Mol Immunol* **17**,
783 113-122 (2020). https://doi.org:10.1038/s41423-019-0359-1

784 7 Stolley, J. M. *et al.* Retrograde migration supplies resident memory T cells to lung-draining
785 LN after influenza infection. *J Exp Med* **217** (2020). https://doi.org:10.1084/jem.20192197

786 8 Kelly, A., Houston, S. A., Sherwood, E., Casulli, J. & Travis, M. A. Regulation of Innate and
787 Adaptive Immunity by TGFbeta. *Adv Immunol* **134**, 137-233 (2017).
788 https://doi.org:10.1016/bs.ai.2017.01.001

789 9 Robertson, I. B. & Rifkin, D. B. Regulation of the Bioavailability of TGF-beta and TGF-beta-
790 Related Proteins. *Cold Spring Harb Perspect Biol* **8** (2016).
791 https://doi.org:10.1101/cshperspect.a021907

792 10 McEntee, C. P., Gunaltay, S. & Travis, M. A. Regulation of barrier immunity and homeostasis
793 by integrin-mediated transforming growth factor beta activation. *Immunology* **160**, 139-148
794 (2020). https://doi.org:10.1111/imm.13162
795 11 Rubtsov, Y. P. *et al.* Regulatory T cell-derived interleukin-10 limits inflammation at
796 environmental interfaces. *Immunity* **28**, 546-558 (2008).
797 https://doi.org:10.1016/j.immuni.2008.02.017
798 12 Worthington, J. J. *et al.* Integrin alphavbeta8-Mediated TGF-beta Activation by Effector
799 Regulatory T Cells Is Essential for Suppression of T-Cell-Mediated Inflammation. *Immunity*
800 **42**, 903-915 (2015). https://doi.org:10.1016/j.immuni.2015.04.012
801 13 Nakawesi, J. *et al.* alphavbeta8 integrin-expression by BATF3-dependent dendritic cells
802 facilitates early IgA responses to Rotavirus. *Mucosal Immunol* **14**, 53-67 (2021).
803 https://doi.org:10.1038/s41385-020-0276-8
804 14 Travis, M. A. *et al.* Loss of integrin alpha(v)beta8 on dendritic cells causes autoimmunity and
805 colitis in mice. *Nature* **449**, 361-365 (2007). https://doi.org:10.1038/nature06110
806 15 Fenton, T. M. *et al.* Inflammatory cues enhance TGFbeta activation by distinct subsets of
807 human intestinal dendritic cells via integrin alphavbeta8. *Mucosal Immunol* **10**, 624-634
808 (2017). https://doi.org:10.1038/mi.2016.94
809 16 Worthington, J. J., Czajkowska, B. I., Melton, A. C. & Travis, M. A. Intestinal dendritic cells
810 specialize to activate transforming growth factor-beta and induce Foxp3+ regulatory T cells
811 via integrin alphavbeta8. *Gastroenterology* **141**, 1802-1812 (2011).
812 https://doi.org:10.1053/j.gastro.2011.06.057
813 17 Lacy-Hulbert, A. *et al.* Ulcerative colitis and autoimmunity induced by loss of myeloid alphav
814 integrins. *Proc Natl Acad Sci U S A* **104**, 15823-15828 (2007).
815 https://doi.org:10.1073/pnas.0707421104

816 18 Paidassi, H. *et al.* Preferential expression of integrin alphavbeta8 promotes generation of
817 regulatory T cells by mouse CD103+ dendritic cells. *Gastroenterology* **141**, 1813-1820 (2011).
818 https://doi.org:10.1053/j.gastro.2011.06.076
819 19 Kelly, A. *et al.* Human monocytes and macrophages regulate immune tolerance via integrin
820 alphavbeta8-mediated TGFbeta activation. *J Exp Med* **215**, 2725-2736 (2018).
821 https://doi.org:10.1084/jem.20171491
822 20 Mohammed, J. *et al.* Stromal cells control the epithelial residence of DCs and memory T cells
823 by regulated activation of TGF-beta. *Nat Immunol* **17**, 414-421 (2016).
824 https://doi.org:10.1038/ni.3396
825 21 Hirai, T. *et al.* Keratinocyte-Mediated Activation of the Cytokine TGF-beta Maintains Skin
826 Recirculating Memory CD8(+) T Cells. *Immunity* **50**, 1249-1261 e1245 (2019).
827 https://doi.org:10.1016/j.immuni.2019.03.002
828 22 Mani, V. *et al.* Migratory DCs activate TGF-beta to precondition naive CD8(+) T cells for
829 tissue-resident memory fate. *Science* **366** (2019). https://doi.org:10.1126/science.aav5728
830 23 McKarns, S. C. & Schwartz, R. H. Distinct effects of TGF-beta 1 on CD4+ and CD8+ T cell
831 survival, division, and IL-2 production: a role for T cell intrinsic Smad3. *J Immunol* **174**, 2071-
832 2083 (2005). https://doi.org:10.4049/jimmunol.174.4.2071
833 24 Laine, A. *et al.* Regulatory T cells promote cancer immune-escape through integrin
834 alphavbeta8-mediated TGF-beta activation. *Nat Commun* **12**, 6228 (2021).
835 https://doi.org:10.1038/s41467-021-26352-2
836 25 Dodagatta-Marri, E. *et al.* Integrin alphavbeta8 on T cells suppresses anti-tumor immunity in
837 multiple models and is a promising target for tumor immunotherapy. *Cell Rep* **36**, 109309
838 (2021). https://doi.org:10.1016/j.celrep.2021.109309
839 26 Takasaka, N. *et al.* Integrin alphavbeta8-expressing tumor cells evade host immunity by
840 regulating TGF-beta activation in immune cells. *JCI Insight* **3** (2018).
841 https://doi.org:10.1172/jci.insight.122591

842 27 Anderson, K. G. *et al.* Intravascular staining for discrimination of vascular and tissue
843 leukocytes. *Nat Protoc* **9**, 209-222 (2014). https://doi.org:10.1038/nprot.2014.005
844 28 Abe, M. *et al.* An assay for transforming growth factor-beta using cells transfected with a
845 plasminogen activator inhibitor-1 promoter-luciferase construct. *Anal Biochem* **216**, 276-284
846 (1994). https://doi.org:10.1006/abio.1994.1042
847 29 Liu, G. *et al.* Platelet activating factor receptor regulates colitis-induced pulmonary
848 inflammation through the NLRP3 inflammasome. *Mucosal Immunol* **12**, 862-873 (2019).
849 https://doi.org:10.1038/s41385-019-0163-3
850 30 Horvat, J. C. *et al.* Neonatal chlamydial infection induces mixed T-cell responses that drive
851 allergic airway disease. *Am J Respir Crit Care Med* **176**, 556-564 (2007).
852 https://doi.org:10.1164/rccm.200607-1005OC
853

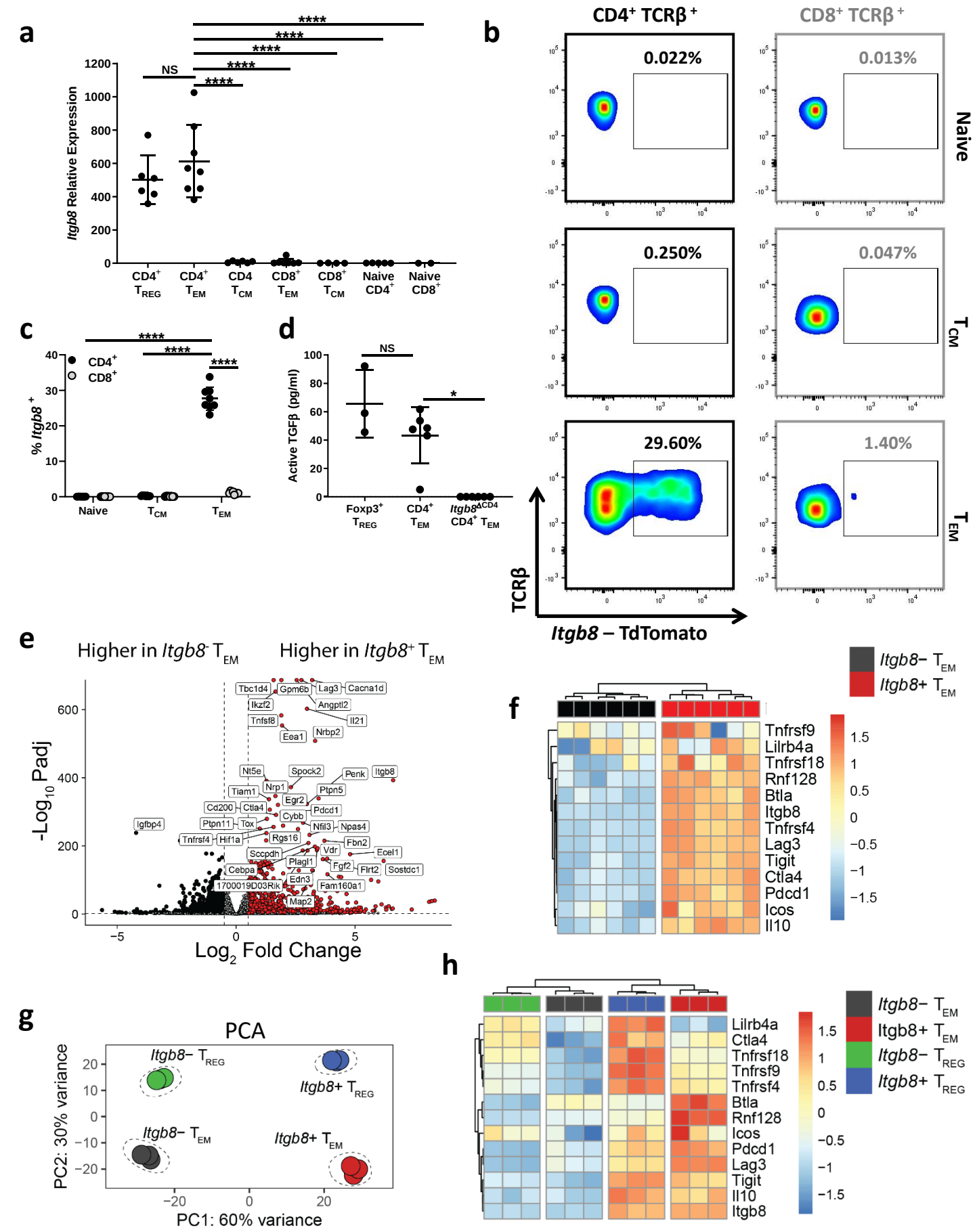
a
Itgb8 Relative Expression
NS
****
CD4+ TREG
CD4+ TEM
CD4 TCM
CD8+ TEM
CD8+ TCM
Naive CD4+
Naive CD8+
b
CD4+ TCRβ+
CD8+ TCRβ+
0.022%
0.013%
Naive
0.250%
0.047%
TCM
29.60%
1.40%
TEM
TCRβ
Itgb8 – TdTomato
c
% Itgb8+
CD4+
CD8+
Naive
TCM
TEM
d
Active TGFβ (pg/ml)
NS
*
Foxp3+ TREG
CD4+ TEM
Itgb8ΔCD4 CD4+ TEM
e
Higher in Itgb8- TEM
Higher in Itgb8+ TEM
-Log10 Padj
Log2 Fold Change
Tbc1d4
Gpm6b
Lag3
Cacna1d
Ikzf2
Angptl2
Tnfsf8
Il21
Eea1
Nrbp2
Nt5e
Spock2
Penk
Itgb8
Tiam1
Nrp1
Ptpn5
Egr2
Cd200
Ctla4
Pdcd1
Cybb
Igfbp4
Ptpn11
Tox
Nfil3
Npas4
Tnfrsf4
Hif1a
Rgs16
Fbn2
Vdr
Ecel1
Sccpdh
Plagl1
Fgf2
Flrt2
Sostdc1
Cebpa
Edn3
1700019D03Rik
Fam160a1
Map2
f
Itgb8− TEM
Itgb8+ TEM
Tnfrsf9
Lilrb4a
Tnfrsf18
Rnf128
Btla
Itgb8
Tnfrsf4
Lag3
Tigit
Ctla4
Pdcd1
Icos
Il10
g
PCA
Itgb8− TREG
Itgb8+ TREG
Itgb8− TEM
Itgb8+ TEM
PC2: 30% variance
PC1: 60% variance
h
Itgb8− TEM
Itgb8+ TEM
Itgb8− TREG
Itgb8+ TREG
Lilrb4a
Ctla4
Tnfrsf18
Tnfrsf9
Tnfrsf4
Btla
Rnf128
Icos
Pdcd1
Lag3
Tigit
Il10
Itgb8

Figure 1

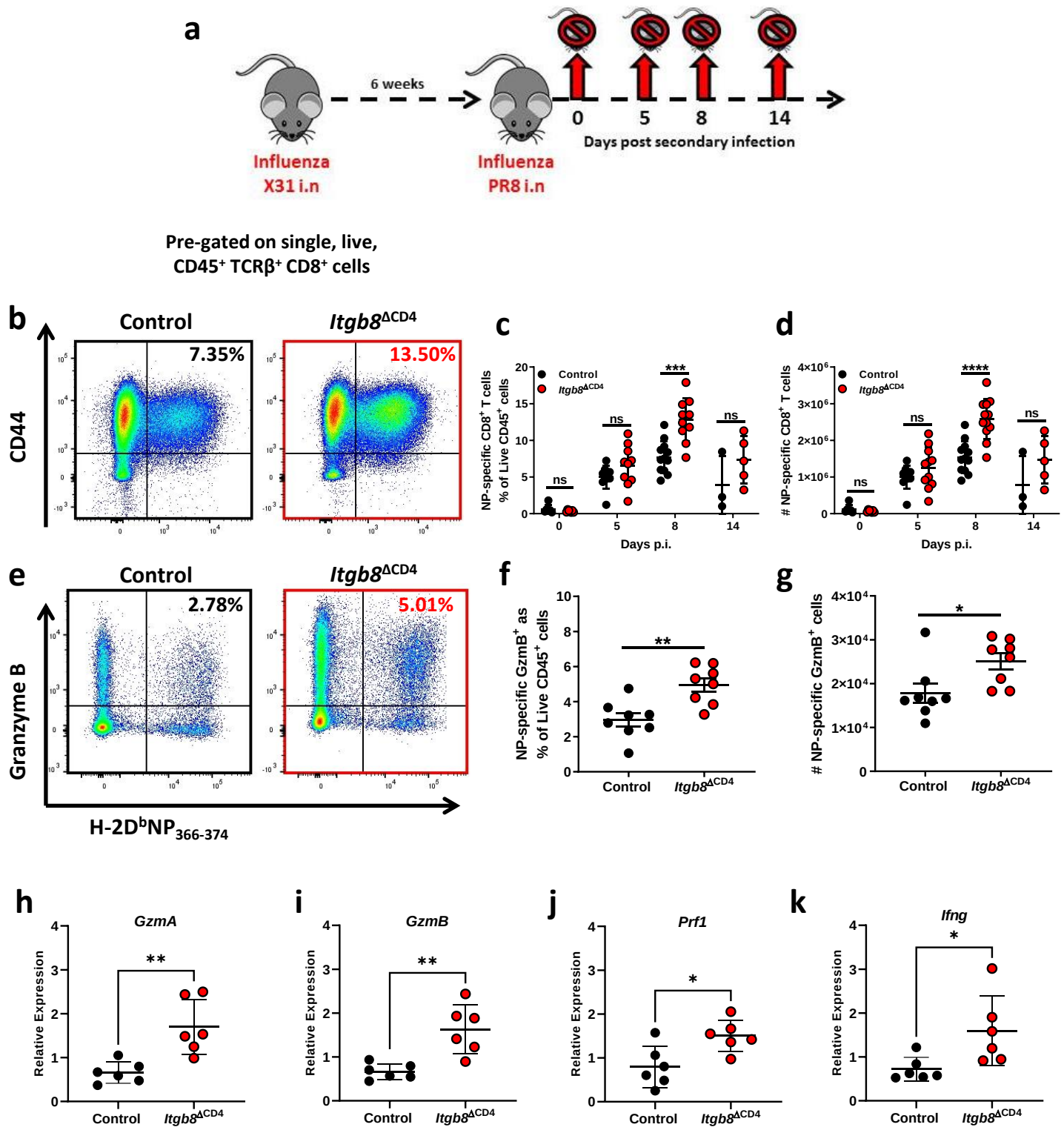
a
6 weeks
Influenza X31 i.n
Influenza PR8 i.n
0
5
8
14
Days post secondary infection
Pre-gated on single, live, CD45+ TCRβ+ CD8+ cells
b
Control
Itgb8ΔCD4
7.35%
13.50%
CD44
c
NP-specific CD8+ T cells % of Live CD45+ cells
Control
Itgb8ΔCD4
ns
***
Days p.i.
d
NP-specific CD8+ T cells
****
e
2.78%
5.01%
Granzyme B
H-2DbNP366-374
f
NP-specific GzmB+ as % of Live CD45+ cells
**
g
NP-specific GzmB+ cells
*
h
GzmA
Relative Expression
i
GzmB
j
Prf1
k
Ifng

Figure 2

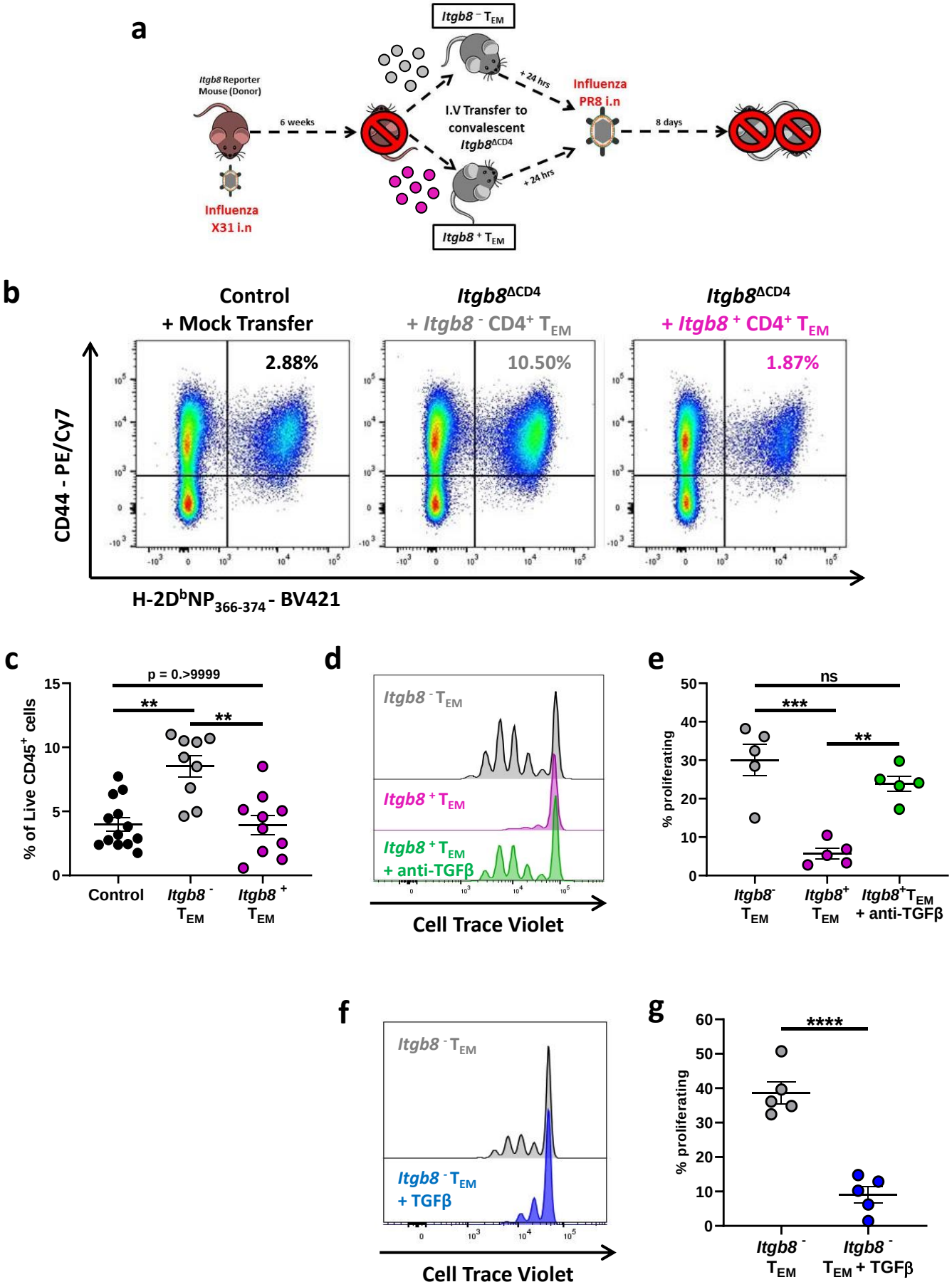
a
Itgb8 Reporter Mouse (Donor)
6 weeks
Influenza X31 i.n
Itgb8 - TEM
Itgb8 + TEM
I.V Transfer to convalescent Itgb8ΔCD4
+ 24 hrs
+ 24 hrs
Influenza PR8 i.n
8 days
b
Control + Mock Transfer
Itgb8ΔCD4 + Itgb8 - CD4+ TEM
Itgb8ΔCD4 + Itgb8 + CD4+ TEM
2.88%
10.50%
1.87%
CD44 - PE/Cy7
H-2DbNP366-374 - BV421
c
p = 0.>9999
**
**
% of Live CD45+ cells
Control
Itgb8 - TEM
Itgb8 + TEM
d
Itgb8 - TEM
Itgb8 + TEM
Itgb8 + TEM + anti-TGFβ
Cell Trace Violet
e
ns
***
**
% proliferating
Itgb8- TEM
Itgb8+ TEM
Itgb8+TEM + anti-TGFβ
f
Itgb8 - TEM
Itgb8 - TEM + TGFβ
Cell Trace Violet
g
****
% proliferating
Itgb8 - TEM
Itgb8 - TEM + TGFβ

Figure 3

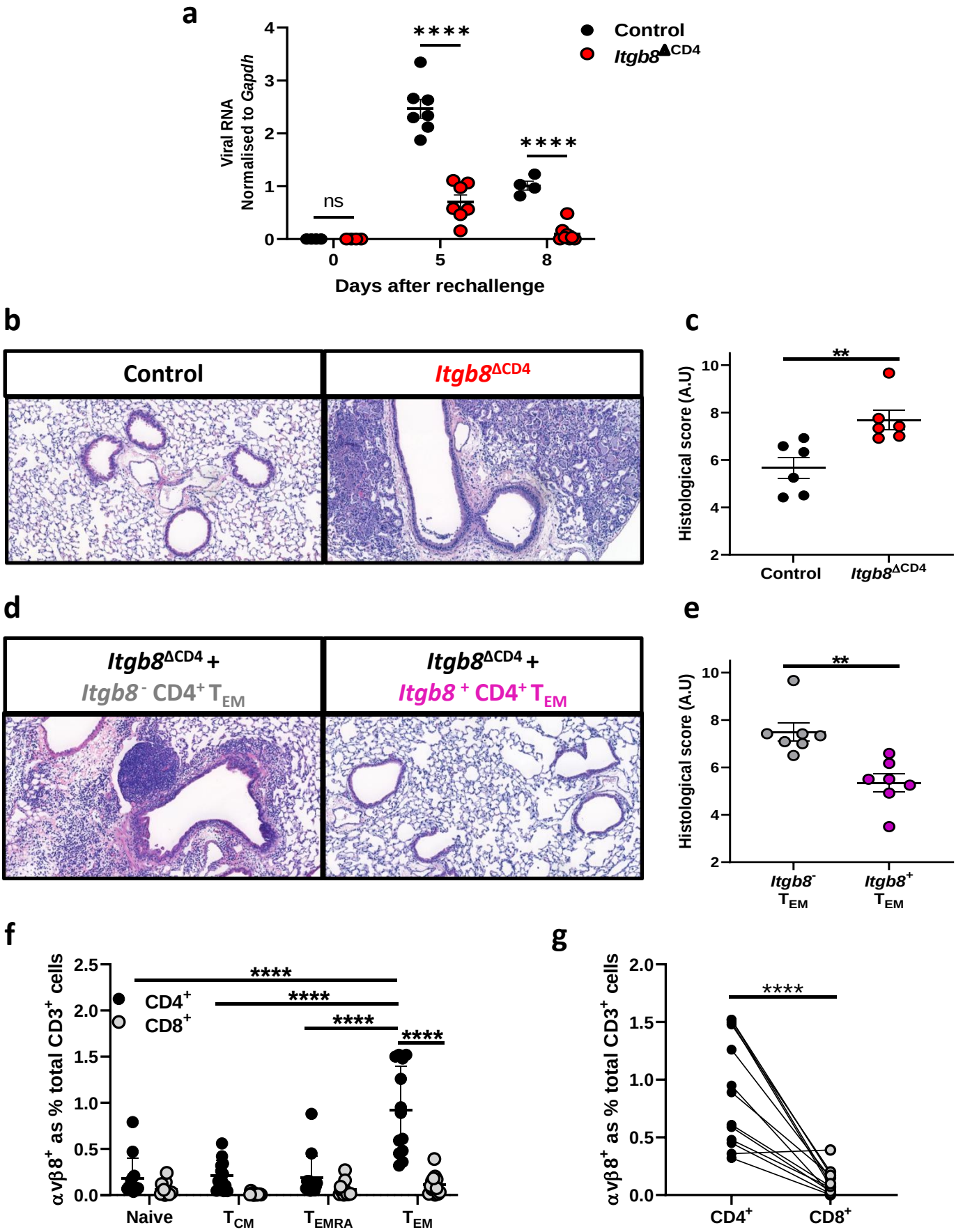
a
Viral RNA Normalised to Gapdh
Days after rechallenge
Control
Itgb8ΔCD4
ns
****
****
b
Control
Itgb8ΔCD4
c
Histological score (A.U)
Control
Itgb8ΔCD4
**
d
Itgb8ΔCD4 +
Itgb8- CD4+ TEM
Itgb8ΔCD4 +
Itgb8 + CD4+ TEM
e
Histological score (A.U)
Itgb8- TEM
Itgb8+ TEM
**
f
αvβ8+ as % total CD3+ cells
CD4+
CD8+
Naive
TCM
TEMRA
TEM
****
g
αvβ8+ as % total CD3+ cells
CD4+
CD8+
****

Figure 4